HOKKAIDO UNIVERSITY

Title	Analysis of the Performance of Thermoelectric Modules Under Concentrated Radiation Heat Flux
Author(s)	Suzuki, Ryosuke; Ito, Keita; Oki, Sae
Citation	Journal of electronic materials, 45(3), 1827-1835 https://doi.org/10.1007/s11664-015-4237-z
Issue Date	2016-03
Doc URL	http://hdl.handle.net/2115/64614
Rights	The final publication is available at Springer via http://dx.doi.org/10.1007/s11664-015-4237-z
Type	article (author version)
File Information	SuzukiItoOki_R10noMark.pdf

Instructions for use

Hokkaido University Collection of Scholarly and Academic Papers : HUSCAP

Analysis of the performance of thermoelectric modules under concentrated radiation heat flux

Ryosuke O. Suzuki*, Keita O. Ito and Sae Oki

Division of Materials Science and Engineering,

Faculty of Engineering, Hokkaido University,

Kita-13, Nishi-8, Kita-ku, Sapporo, Hokkaido 060-8628 Japan

**e-mail: rsuzuki@eng.hokudai.ac.jp*

Abstract

The concentration of solar radiation by either the lens or the mirror is one of the options for practical utilization of light to obtain higher temperature. However, it is difficult to maintain high temperature on the hot side of the module due to solar diurnal motion. This study evaluates the influence of the thermoelectric (TE) output by the optical light concentration. Three-dimensional partial differential equations describing heat balance and TE phenomena were simultaneously solved by applying the numerical method, and the temperature distribution in the whole TE module as well as the current density were simulated. It was shown that the three models of light concentration on a single TE module (BiTe based, 4 legs having dimensions of 10*10*10 mm) generate a similar

output at the external load. This happens because the long leg becomes a large thermal resistance, and because the alumina plate (1mm thick) with a high thermal conductivity covers the top of TE modules. The homogenized temperature at the hot junctions generates the similar output at all three models, when the cold terminals were kept at constant temperature.

Keywords;

Thermoelectric generation, solar light concentration, numerical simulation, heat transfer.

1. Introduction

Thermoelectric (TE) power generation from the solar light has been examined as a desired method to use the environmentally friendly energy resource [1-13], and the high temperature generated by light concentration using either the mirrors [1,3-6,8] or the lenses [11-13] was applied to heat one side of TE module. However, it is mechanically difficult to track the solar diurnal motion and to focus the concentrated light on a certain point of the TE module surface at any time during the day [3,11]. In order to minimize the mechanical limitation of optical lens, the authors proposed the utilization of water lens, which can adjust the focal length by its shape change [11-13]. The heat concentration ratio from the solar ray by water lens usually remains lower than 100, even when some specific conditions are set at their best values [11,12]. The ratio by the other methods such as lens and mirror can become as large as 100, but these high ratios are hardly kept for a long time[1,3-6], and the solar ray heats only a narrow specific area of TE module surface.

This paper assumes a realistic case that the concentrated light is radiated on a certain area, not on a mathematically single point. It is important to know how much solar radiation we should effectively accumulate on a certain finite area, and then how much TE power we can generate by a certain temperature difference. Because the solar light heats the upper surface of a TE module consisting of a large number of TE elements, we will properly define the area where

47 the light is concentrated as the best working receiver.

48 For the evaluation of electrical power expected from a single TE module, it is necessary to
49 solve the temperature distribution governing equations in the TE module. Although we may
50 analytically solve only the one-dimensional differential equation for heat transfer in a single
51 module [7,9], three-dimensional solutions are required by considering the surface area and the
52 depth[8,10,11,13-15]. Moreover, in case of a high power generation, the Peltier cooling due to the
53 generated current decreases the TE performance. Therefore, the precise evaluation of
54 performance from the TE module is needed in order to consider the cooling effect caused by
55 Peltier effect as well as the heating effect caused by Joule exothermic heat.

56 Recently, the computer numerical simulations have been reported which showed the
57 predicted three-dimensional temperature profiles in the TE module, and assessed the achievable
58 TE performances [10,12-22]. The authors have also developed the software which combines the
59 heat transfer from the thermal fluids and the TE phenomena [13,16,18-22]. Temperature distribution,
60 thermal electromotive force (EMF), electric potential and current density have been successfully
61 evaluated in three-dimensional space. For example, the TE output power using the thermal
62 fluids [15,18,19] was analysed, and the shape of TE element was optimized by the assistance of that
63 software [20-22]. Similar mathematic approaches were applied, for example, to the system design
64 of the TE generators [21, 23,24].

Usually the TE performances were analysed at a given temperature difference, and at the uniform heat flow [25,26]. The local heating such as one in the case of light concentration was not often considered [1-9]. Inhomogeneous distribution of temperature on the receiver may be homogenized due to thermal heat diffusion through a thick substrate. However, the thicker plate becomes the stronger barrier for the heat transfer, and the hot terminal temperature of TE leg decreases with increasing thickness. This may suppress the TE output. A suitable thickness of receiving plate must be optimized to obtain the best performance of the TE module.

This study will report the details of the analysis of three-dimensional heat transfer for the case in which the radiation heat is locally concentrated on a part of the TE module surface. The effects of inhomogeneous temperature profile in either two-dimensional area or in three-dimensional space on TE power are also described. The relationship between the inhomogeneous profile on the top surface and the generation performances is studied. An assumption was often examined that the two flat surfaces of TE module are homogeneously kept at the two different constant temperatures. It is noted, however, that this study will give the inhomogeneous temperature distribution under the concentrated heat radiation condition. The light reflection and heat radiation from the surfaces are neglected for simplicity.

2. Methods

In a TE element, the inhomogeneous heat flow as well as the inhomogeneous current density are estimated under the inhomogeneous thermal input. Also a close relationship exists between the temperature and the current density. We will simultaneously solve two differential equations describing the heat transfer and the principle of electric charge conservation in three-dimensional space [10,12-16]. Because the detailed procedure was already reported [14-16], a brief introduction is given here.

First, the heat conduction equation is written as,

$$\nabla \cdot \left(-\kappa \nabla T\right) = \frac{|\mathbf{J}|^2}{\sigma} - T\mathbf{J} \cdot \nabla S \qquad (1)$$

where **J** and T are current density and temperature. Three thermoelectric properties of thermal conductivity, κ, electric conductivity, σ, and Seebeck coefficient, S, are not dependent on the crystalline direction, but are dependent on temperature. The left side of eq.(1) represents the heat transfer due to Fourier law. The first and second terms of the right-hand side of eq.(1) take into account Joule heat and Thompson effect, respectively.

Second, **J** is produced from the increment of voltage due to Seebeck effect and the voltage drop due to Ohm law, and can be expressed in the following form:

$$\mathbf{J} = -S\sigma\nabla T - \sigma\nabla V \qquad (2)$$

Current density in the steady state can be derived from the principle of electric charge conservation as,

$$\nabla \cdot \mathbf{J} = 0 \tag{3}$$

By combining eq. (2) and (3), the governing equation of electric field distribution is derived as,

$$0 = \nabla \cdot \left(\sigma \nabla V + S \sigma \nabla T \right) \tag{4}$$

Eq. (1) and (4) can be solved simultaneously under two boundary conditions to obtain the electric potential distribution, $V(x,y,z)$, and the temperature distribution, $T(x,y,z)$.

We used the commercially available software, ANSYS FLUENT, which is computational fluid dynamics (CFD) numerical software based on the finite volume method. The thermoelectric behaviours were analysed by introducing our original functions to solve eq.(1) and (4) [14-16]. The temperature dependence of thermoelectric properties is taken into account by referring to the material data set through the original users defined functions (UDF) in FLUENT. The current density was derived from the gradient of voltage and temperature.

Fig. 1 shows the flow-chart used in numerical analysis. The temperature $T(x, y, z)$, voltage $V(x, y, z)$ and the voltage drop due to ohmic resistance, $V_{ohm}(x, y, z)$ are given as the initial conditions, while the thermoelectric behaviours, the exothermal heat and endothermal heat are evaluated. Next, the temperature and voltage profiles are obtained by solving eq. (1) and (4). From these solutions, the voltage over all the modules is revised. By iteration procedure, a set of T, V and V_{ohm} values was given. These variables at a terminal were set the constant at a boundary, and the values at the other terminal were not constrained. The calculated distribution at the TE

terminal is averaged for the representing value of the model. Thompson heat is a heat generated as the gradient of Seebeck coefficient, and its calculation with eq.(4) doubles the calculation of Peltier heat at the junctions of two different materials. For the precise evaluation of Peltier cooling, therefore, the mesh size close to the boundaries is set fine.

3. Modelling of TE module

Conventional Π type module is assumed. The material properties for the module are listed in Table I [27]. Bi_2Te_3 is taken as an example of TE elements and its thermoelectric properties are listed in Table II [28].

The substrates of the Π-type TE module surface should mechanically support the mass of TE elements. The thickness of dense alumina substrates is chosen to be 1.00 mm because of mechanical strength necessary to hold the mass of TE module. As shown in Fig. 2, 4 pieces of TE elements are imbedded in the alumina substrate. It is noted that the dense alumina has a relatively good thermal conductivity. The electrodes are copper plates (0.5 mm thick) and all the TE elements are 10.0 mm cube. These sizes are not far from the dimensions at the modules commercially available in the market. It looks a little fat element, but this dimension can be thought that it can represent a thermopile consisting of several tens pairs of TE elements. This simulation will give a fundamental step for more precise analysis in future.

137 The contact resistance at all junctions is taken into account in this model. Thermal resistance
138 between the alumina substrate and the electrode can be decreased by using a thermal conductive
139 grease. The thickness of grease is set 80 μm because too thick pasting produces a large thermal
140 resistance. The thermal and electric resistances at the contact between the electrode and the TE
141 material are assumed to be $10^{-4}m^2KW^{-1}$ and $10^{-11}\Omega m^2$, respectively, as reported for the good
142 junctions welded by the solder [29].

143 The concentration of the solar light is assumed in the following way; the ray is concentrated
144 by a lens and irradiates vertically on the module's surface, and the radiated light homogeneously
145 heats the upper surface of TE module, as shown in Fig. 3. Three models, I, II and III, are
146 considered; the ray is concentrated on 1x1, 5x5 and 30x30 mm square, as shown in Fig.3 (a), (b)
147 and (c), respectively. The condition of the model I corresponds to that concentrated very sharply
148 by a lens with a precise geometry control, and that of the model III is the mild case such as
149 water lens concentration [11]. The studied radiated area was assumed to be the square by using a
150 Fresnel lens. Without loss of generality, this assumption avoids the technical problem that a
151 certain amount of numerical error is generated when a circular light radiates the square meshes
152 on the surface of TE module. A total energy for the light radiation for all three models is
153 commonly set to be 9.00 W. The heat flux at the irradiated top surface is $9MWm^{-2}$, 360 kWm^{-2}
154 and 10 kWm^{-2}, for models I, II and III, respectively. It should be noted that even the weak heat

flux for the model III is 10 times larger than the natural solar radiation density to the earth, 1 kW/m^2. These conditions are assumed to be suitable for generating the temperature difference between two terminals of TE elements. All the input heat is assumed to be absorbed in the alumina plate. In order to examine the effects of a constant heat flux and to simplify the calculations, the cold surface of alumina plate was kept at 300 K, as one of the fundamental assumptions for calculation. The heat radiation from the TE module is neglected.

4. Results and Discussion

4.1 Temperature distribution

After the three-dimensional calculations, the temperature distributions in the TE module were obtained and are shown in Fig. 4. The temperature on the top surface of alumina substrate in the model I exceeded 600 K at the irradiated area, as shown in Fig.4 (a). The central portion of the top surface in the model II was higher than the other surrounding area, as shown in Fig.4 (b). The temperature of the top surface in the model III became more homogeneous, as shown in Fig. 4(c). The central area of the top surface in this model III, especially the areas where the copper electrodes are attached to the opposite side of alumina substrate, were cooler than the substrate edges. This is due to the strong heat transfer through the electrodes and TE elements to the colder surface of TE module. It should be noted that the temperature at the cold surface was fixed at 300K, as the boundary condition necessary to solve the system of differential equations.

The upper surface temperature of the copper electrodes are shown in Fig. 4 (d), (e) and (f) by removing the alumina substrate for demonstration. The temperature profiles at the upper surface of electrodes are relatively homogeneous and similar to one another in three models. This means that the alumina substrate only 1.00 mm thick is effective for thermal diffusion along the horizontal directions, and that this thickness is good for homogeneous temperature profile. Namely, the light concentration on a special point of the TE module does not play an efficient role in heating the TE elements below the alumina substrate. The maximum temperature at the hot terminals of TE elements does not reach the melting point of solder at the junctions.

Inside the TE modules, the temperature profiles change linearly with the height, because a steady state is established. The cooling to keep the cold surface at 300 K could effectively extract the input heat from the hot surface, because the amounts of extracted heat at the cold surface are almost equivalent for these three models, as shown in temperature profiles. This is because the homogeneous temperature distributions in the hot alumina substrates and the similar temperature profiles in TE legs are commonly generated in three models. The assumption of 300 K mean a mild cooling not to affect the temperature difference between the hot and cold junctions.

192 **4.2 Power generation**

193 By connecting these TE modules with the external load, we can get the TE output there. The
194 simulation can evaluate the circuit current by summing the current densities at the connections
195 with the external resistance. The voltage generated at the two terminals of the external
196 resistance is also calculated, and the TE output power, *P*, is evaluated by multiplying the current
197 and voltage. Fig. 5 shows the analysed output power as a function of current. The obtained TE
198 power commonly shows the maximum, which is the well-known phenomenon in TE power
199 generation. Three models showed the equivalent output power: the power does not depend on
200 the degree of light concentration. The maximum power is evaluated as 431 mW at 7A, where
201 the efficiency is calculated as 4.79 %.

202 For the cases in which the maximum output power can be obtained, the temperature
203 distributions are shown in Fig. 6. They are almost identical for the models I and II, as shown in
204 Fig. 6(a) and (b), respectively, where the light was commonly concentrated to the centre of the
205 module. When the light radiates the top surface of TE module homogeneously, as it is assumed
206 for the model III, it is natural that the temperature distribution is homogeneous (Fig. 6(c)), and
207 that temperature at the same height is the same in any model.

208 The detailed temperature distributions on the top surface of alumina plate, on the upper
209 surface of the upper electrode, on the surface of the upper terminal and at the two side edges of

TE elements are shown in Fig. 7(a), (b), (c) and Fig. 8, respectively, where the maximum output power is generated at the model I. The centre of top surface of the alumina plate is heated highly, and the inhomogeneous and unsymmetrical profiles can be seen at Fig. 7(a). Due to cooling from the TE elements the four edges of alumina plate is cooled. The inhomogeneity at the alumina plate is smeared further at the copper electrodes, as shown in Fig.7(b), where the temperature difference at the upper surface is smaller than 10 K two-dimensionally. It is interesting that the central portions of the electrode is hotter than the edges, as shown in Fig.7(b), and that the surface temperatures of alumina plate are also hotter at these positions. The temperature inhomogeneity at the TE terminals is much smaller and almost homogeneous, as shown in Fig.7 (c). In addition to the alumina plate (1 mm thick), the copper plates (0.5 mm thick) are also contributed for homogeneous temperature profile.

Fig. 8 shows the temperature distributions at the side edges of TE element. T_A and T_B are the temperatures calculated at the inner and outer edges, respectively, as illustrated in Fig. 8. The temperature profiles in the alumina plates and copper electrodes at the same horizontal (X-Y) positions are also shown in Fig. 8. Because of good thermal conductivities in alumina and copper, the temperature gradients in these materials are almost flat against height, and the major temperature drop is given to the TE elements. The thermal conductive grease and the welding at the junctions do not give any significant temperature drop in this simulation. At the steady state

between two terminals, if the TE terminals are kept at the constant temperatures, the temperature linearly decreases from the hot terminal to the cold one. Because the temperature distribution at the hot alumina surface exists here, however, the hot terminal temperature of TE element are not fixed.

It is noted that the temperature drop in the TE materials looks linear at both T_A and T_B. In order to examine the linearity of temperature drop, the difference of T_A and T_B is defined as ΔT and evaluated as shown in Fig. 8. If the both T_A and T_B are perfectly linear, ΔT should be linear. The weak temperature dependency of the material properties as listed in Table II does not form this parabolic behavior, and this curious behavior of ΔT may suggest the slant heat transfer in TE element, as reported previously [20,21].

Because this study neglected the radiation from the surfaces, it should be considered for the more detailed analysis. This effect may strongly appear in the area heated at the higher temperatures, because the radiation is proportional with the function of T^4. Therefore, the radiation effect is limited at these high-temperature area. The heat conduction at the lower temperature area is not affected from the heat radiation at the TE side surfaces.

The current densities calculated for these cases are shown in Fig. 9. They are high at the central part of the upper electrodes because the current through the TE elements flows into the electrode through the junctions, and because it increases from an edge of the electrode to

246 another edge of the TE element. The current density is constant through the area between two
247 TE elements, where no TE elements exist below the centre of the electrode. This constant
248 current density at the lower electrodes is also partially seen in Fig. 9, marked with orange colour.
249 The current densities are identical anywhere in the TE elements at a certain model, and also
250 identical in all three models. It is also natural that the Seebeck effect is caused homogeneously
251 inside the TE elements, because the temperature distributions are homogeneous and identical.
252 Consequently, the current density becomes identical.

253 These analyses reveal that the input heat can be diffused out in the alumina enough thick to
254 remove any inhomogeneous temperature distribution, even if the significant temperature
255 distribution exists at the upstream on the hot substrate. Then, the temperature profiles in the TE
256 elements become identical in all three models. Resultantly, the TE output power is not affected
257 by the light concentration, when the alumina plate is thicker than 1.00 mm.

258

259 **4.3 Concentration of radiation heat**

260 Fig.10 shows some variations of TE modules for solar light power generation. When the
261 radiation and thermal conduction of air can be neglected, and when the heat resistance of TE
262 element is sufficiently large, the size of alumina plate can be expanded as shown in Fig. 10(a)
263 comparing to the model II and III shown in Fig. 3. The effect of light concentration on TE
264 output was very weak as shown in Fig. 6, and we may radiate the solar light on the alumina

plate without any concentration, as illustrated in Fig. 10(b). When the alumina plate is large, the TE elements can be set at the corners of the alumina plate for mechanical stability, as shown in Fig. 10(c). The large alumina plate and the copper electrodes diffuse the obtained heat homogeneously, and they pass it to the TE elements. This fundamental concept in this work can be applied in various designs in future. For more precise analysis, the effects of heat reflection, radiation and thermal conduction to the surrounding environment should be taken into account of.

5 Summary

The temperature distribution in the Π-type TE module (consisting of 4 TE elements) was simulated. This computer simulation was based on the heat balance and TE phenomena. When the light is concentrated on a point of TE top surface, the isothermal contour of temperature distribution look like a circle on the top surface. However, these inhomogeneous profiles become equalized by passing the heat into the thick alumina substrate, and the homogeneous heat flows after passing in the copper electrodes are passing through the TE elements. The temperature distribution is homogeneous at the same height, and it is almost linear with height of TE element. It was found that the output powers from three analysed models are identical. Due to the slow thermal diffusion inside the alumina plate, the effect of the light concentration

is smeared out.

In case of TE power generation by receiving the solar light, the light concentration ratio is not so serious to enhance TE performance. Due to homogenization of temperature profile at the alumina plate, it is not necessary to use a high degree of light concentration by the lens.

For more precise analysis, the effects of heat reflection, radiation and thermal conduction to the surrounding environment should be taken into account of.

Acknowledgements

The authors thank Dr. Xiang-ning Meng at Northeastern University, China, Dr. Ryoji Funahashi at AIST Kansai, Japan, Dr. Shungo Natsui and Prof. Dr. Krzysztof Fitzner at Hokkaido University, for their kind advices. The program used here was originally coded by Dr. Min Chen at Aalborg University, Denmark, and Mr. Takeyuki Fujisaka at Hokkaido University (now at Nippon Steel & Sumitomo Metal Co., Japan). It was modified to adjust with this paper. This work is financially supported in part by Grant-in-Aid for Challenging Exploratory Research (JSPS, Nos. 26630490 and 24656574).

References

1) H.J. Goldsmid, J. E. Giutronich and M. M. Kaila, Solar Energy, 24 (1980) 435-440.

2) Jincan Chen, J. Appl. Phys. 79 (5) (1996) 2717-2721.

3) Narong Vatcharasathien, Jongjit Hirunlabh, Joseph Khedari and Michel Daguenet, Intern. J. Sustainable Energy, 24 (3) (2005) 115-127.

4) Clemens Suter, Petr Tomeš, Anke Weidenkaff and Aldo Steinfeld, Materials, 3 (2010) 2735-2752.

5) R. R. Amatya and R.J. Ram, J. Electr. Mater. 39 (9) (2010) 1725-1740.

6) Peng Li, Lanlan Cai, Pengcheng Zhai, Xinfeng Tang, Qingjie Zhang and M. Niino, J. Electr. Mater., 39 (9) (2010) 1522-1530.

7) Daniel Kraemer, Bed Poudel, Hsien-Ping Feng, J. Christopher Caylor, Bo Yu, Xiao Yan,Yi Ma, Xiaowei Wang, Dezhi Wang, Andrew Muto, Kenneth McEnaney, Matteo Chiesa, Zhifeng Ren and Gang Chen, Nature Materials, 10 [July] (2011) 532-538.

8) Clemens Suter, Petr Tomeš, Anke Weidenkaff and Aldo Steinfeld, Solar Energy, 85, (2011), 1511–1518.

9) Kenneth McEnaney, Daniel Kraemer, Zhifeng Ren, and Gang Chen: *J. Appl. Phys.*, 110, (2011), 074502.

10) Jinsheng Xiao, Tianqi Yang, Peng Li, Pengcheng Zhai and Qingjie Zhang, Appl. Energy, 93,

319 (2012), 33–38.

320 11) Ryosuke O. Suzuki, Atsushi Nakagawa, Hongtao Sui and Takeyuki Fujisaka, J. Electr.

321 Mater., 42 (7) (2013) 1960-1965.

322 12) Keita O. Ito, Hongtao Sui, Hidetoshi Hakozaki, Hiroshi Kinoshita and Ryosuke O. Suzuki, J.

323 Electr. Mater., 43 (6) (2014) 2086-2093.

324 13) Ryosuke O. Suzuki, Takeyuki Fujisaka, Keita Ito, Xiangning Meng and Hong-tao Sui, J.

325 Electr. Mater. 44 (1) (2015) 348-355.

326 14) Elena E. Antonova and David C. Looan, Proc. 24th Intern. Conf. on Thermoelectrics

327 (ICT2005), (19-23 June 2005) The Institute of Electrical and Electronics Engineers (IEEE),

328 Piscataway, NJ, USA (2005) 200-203.

329 15) Min Chen, Lasse A. Rosendahl and Thomas Condra, Inter. J. Heat and Mass Transfer, 54,

330 (1-3) (2011) 345–355.

331 16) Takeyuki Fujisaka and Ryosuke O. Suzuki, Proc. IECON 2012 - 38th Annual Conference on

332 IEEE Industrial Electronics Society, (25-28 Oct., 2012, Montreal, Canada), The Institute of

333 Electrical and Electronics Engineers (IEEE) , Piscataway, NJ, USA, (2012) 5868-5872.

334 17) Bongkyun Jang, Seungwoo Han and Jeong-Yup Kim, Microelectric Engg., 88 (2011)

335 775-778.

336 18) Ryosuke O. Suzuki, Yuto Sasaki, Takeyuki Fujisaka and Min Chen, J. Electr. Mater., 41 (6)

337 (2012) 1766-1770.

338 19) Ryosuke O. Suzuki, Yuto Sasaki, Takeyuki Fjisaka and Min Chen, Proc. IECON 2012 - 38th

339 Annual Conference on IEEE Industrial Electronics Society, (25-28 Oct., 2012, Montreal,

340 Canada), The Institute of Electrical and Electronics Engineers (IEEE) , Piscataway, NJ, USA,

341 (2012) 5868-5872.

342 20) Xiangning Meng, Takeyuki Fujisaka, Keita O. Ito and Ryosuke O. Suzuki, Mater. Trans., 55

343 (8) (2014) 1219-1225.

344 21) Xiangning Meng and Ryosuke O. Suzuki, J. Electr. Mater., 44 (6) (2015) 1469-1476.

345 22) Takeyuki Fujisaka, Hongtao Sui and Ryosuke O. Suzuki, J. Electr. Mater., 42 (7) (2013)

346 1688-1696.

347 23) Jiin-Yuh Jang and Ying-Chi Tsai, Appl. Therm. Engg., 51 (2013) 677-689.

348 24) Hua Tian, Xiuxiu Sun, Qi Jia, Xingyu Liang, Gequn Shu, Xu Wang, Energy, 84 (2015)

349 121-130.

350 25) Katsutoshi Ono and Ryosuke O. Suzuki, J. Metals, Dec. (1998) 49-51.

351 26) Ryosuke O. Suzuki and Daisuke Tanaka, J. Power Sources, 122 [2] (2003) 201-209.

352 27) The Japan Society of Mechanical Engineering (JSME), “Standard values of heat transfer

353 engineering”, ver.4, 1986, JSME, Tokyo.

354 28) European Thermodynamics Limited, “Datasheet: Thermoelectric Power Generator”

(GM200-71-14-16) Leicester, UK (2014).

29) Yasuhiko Mori, in “Handbook of Thermoelctric Conversion Technology”, ed. by T. Kajikawa, NTS, Tokyo, 2008, pp.400-405.

Table captions

Table I Material property for simulation.[27)]

Table II Temperature dependencies of material properties (T is temperature in K).[28)]

Figure captions

Fig.1 Workflow of the numerical calculation.

Fig.2 Illustration of the studied module.

Fig.3 Simulation models, I (a), II (b) and III (c), for heating with concentrated light.

Fig.4 Temperature profiles on the surface of TE elements. (a)-(c): on the upper surface of alumina plate. (d)-(f): the alumina plate is removed. (a) and (d) are for Model I, (b) and (e) for Model II, and (f) and (c) for Model III.

Fig.5 *I-P* curves when the limited area was heated by radiation. The size of irradiated area is shown. (a), (b) and (c) correspond to the model I, II and III, respectively.

Fig.6 Temperature profiles when the maximum output powers generated. (a), (b) and (c) correspond to the model I, II and III, respectively.

Fig.7 Temperature distributions on (a) top surface of alumina plate, (b) upper surface of electrodes, and (c) upper surfaces of TE elements, when the maximum output power generated at the model I.

Fig.8 Temperature distributions on the two side edges of TE elements, when the maximum output power generated at the model I. T_A and T_B are the temperatures at the inner and outer edges (see Fig.7(c)), and the temperature difference between them, ΔT, is shown as a function of height.

382 Fig.9 Profiles of current density when the maximum output powers generated. (a), (b) and (c)

383 correspond to the model I, II and III, respectively.

384 Fig.10 Illustration of TE modules for solar light power generation, where their maximum output

385 powers are expected to be equivalent with the TE module as shown in Fig. 3(b).

386

Table I Material property for simulation.[27)]

	Seebeck coefficient S [μV/K]	Electric conductivity σ [10^5S/m]	Thermal conductivity κ [W/(m·K)]
Cu	1.83	640	398
Al_2O_3	–	–	36
Grease	–	–	20

Table II Temperature dependencies of material properties (T is temperature in K). [28)]

	P-type element	N-type element
Thermal conductivity, λ [W/ (m·K)]	0.00003615587^2 $-0.026351342T+6.22162$	$0.0000334545T^2$ $-0.023350303T+5.606333$
Seebeck coefficient, S [V/K]	$(-0.0036380957^2$ $+2.74380952T-296.214286)\times10^{-6}$	$(0.00153073T^2$ $-1.08058874T-28.338095)\times10^{-6}$
Electrical conductivity, σ [Sm]	$(0.015601732T^2$ $-15.708052T+4466.38095)\times10^2$	$(0.01057143T^2$ $-10.16048T+3113.71429)\times10^{-6}$

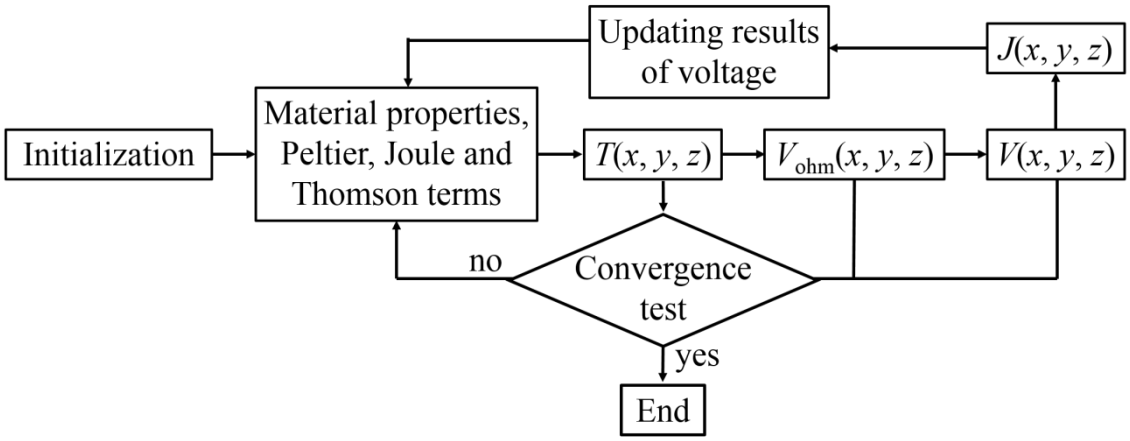

Fig.1 Workflow of the numerical calculation.

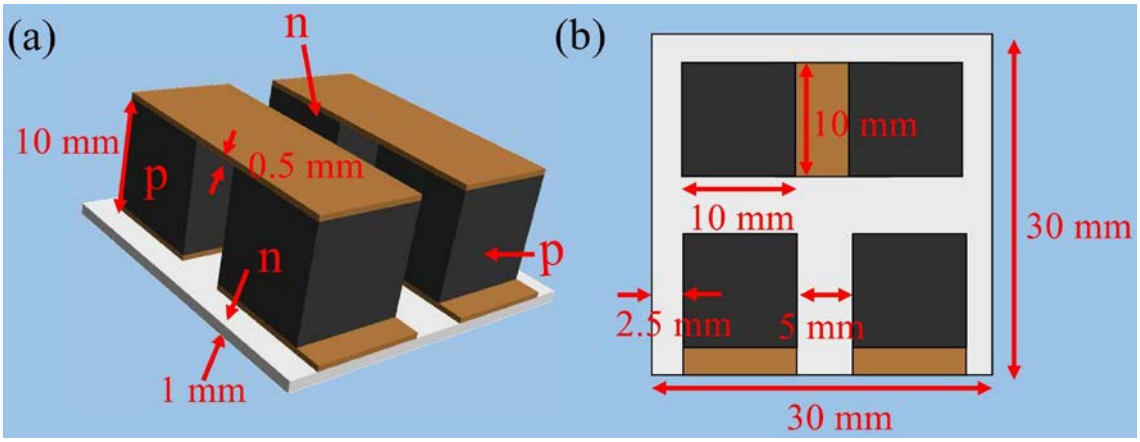

Fig.2 Illustration of the studied module.

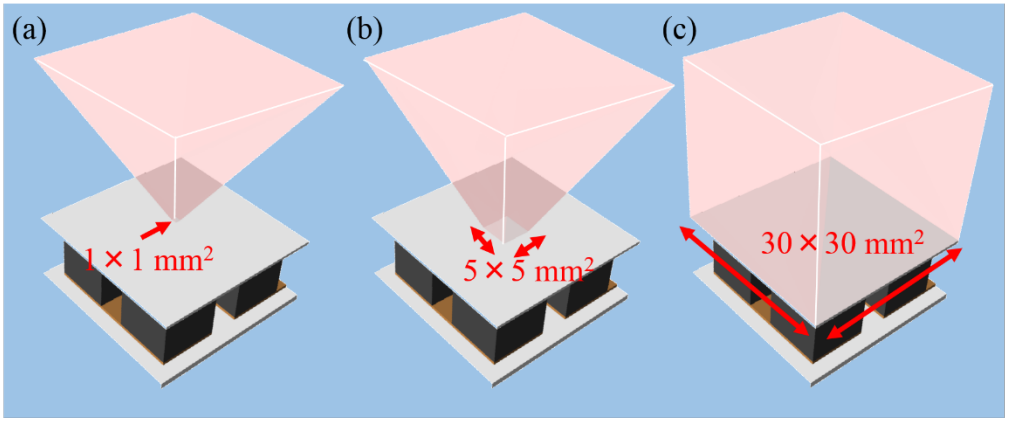

405

406

407 Fig.3 Simulation models, I (a), II (b) and III (c), for heating with concentrated light.

408

409

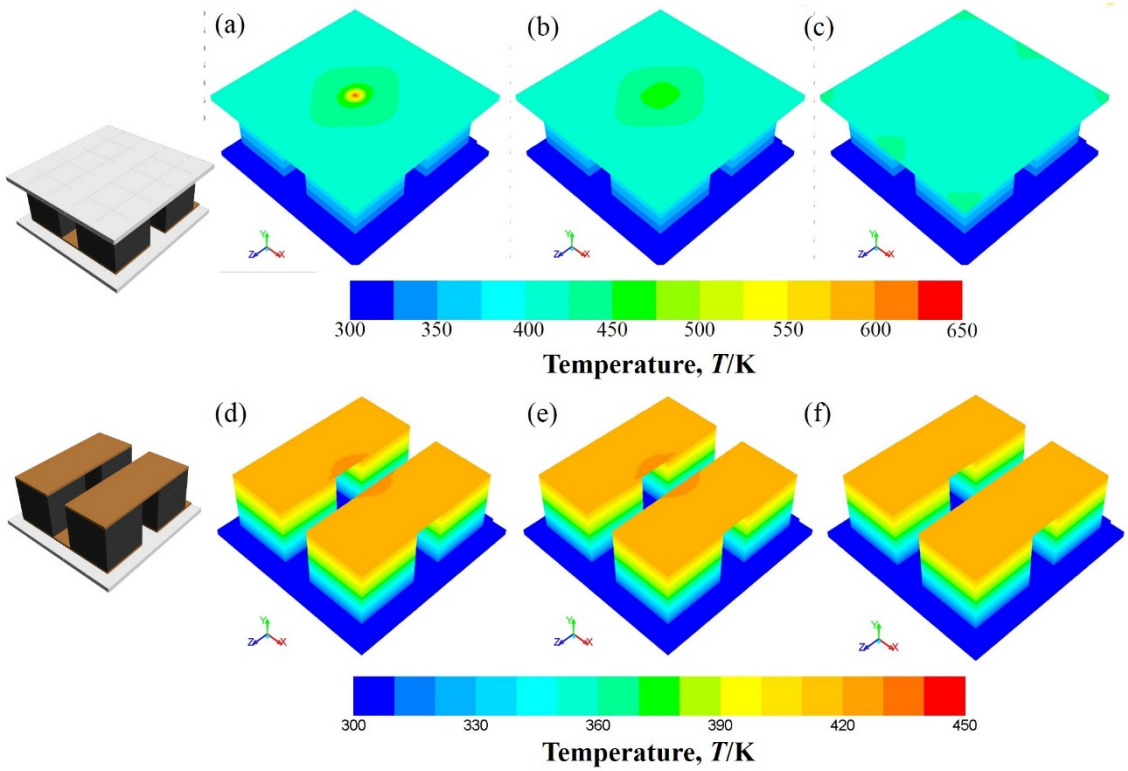

410

411

412 Fig.4 Temperature profiles on the surface of TE elements. (a)-(c): on the upper surface of
413 alumina plate. (d)-(f): the alumina plate is removed. (a) and (d) are for Model I, (b) and (e) for
414 Model II, and (f) and (c) for Model III.

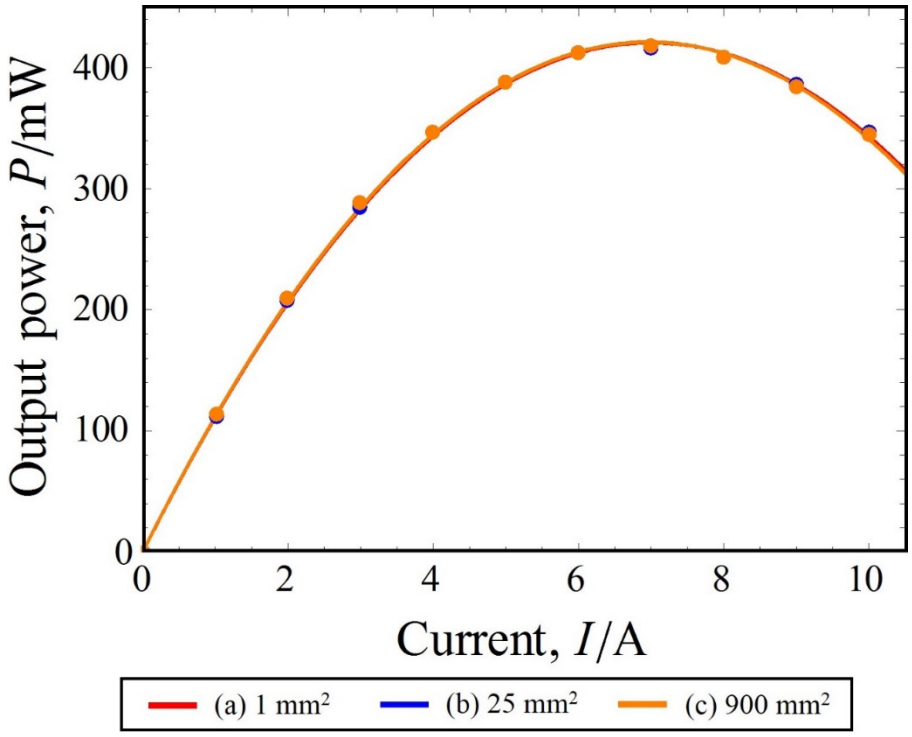

Fig.5 *I-P* curves when the limited area was heated by radiation. The size of irradiated area is shown. (a), (b) and (c) correspond to the model I, II and III, respectively.

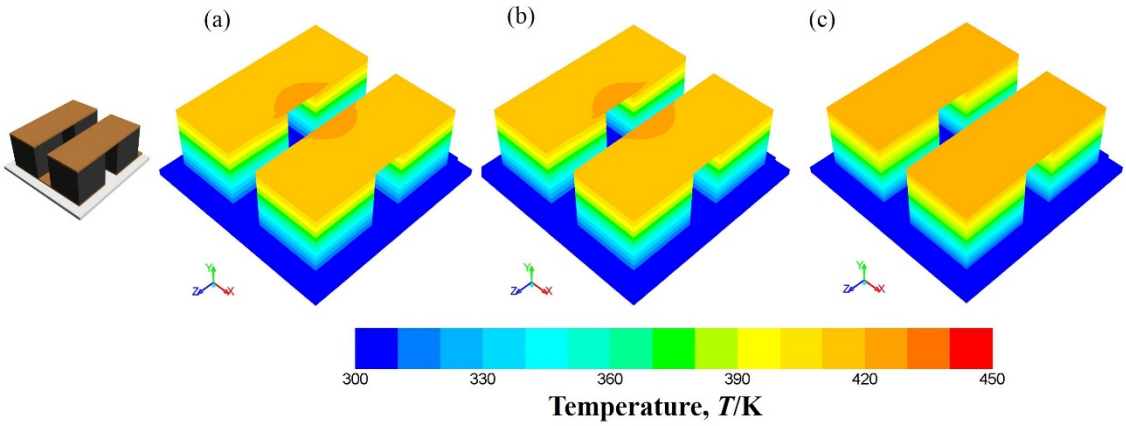

Fig.6 Temperature profiles when the maximum output powers generated. (a), (b) and (c) correspond to the model I, II and III, respectively.

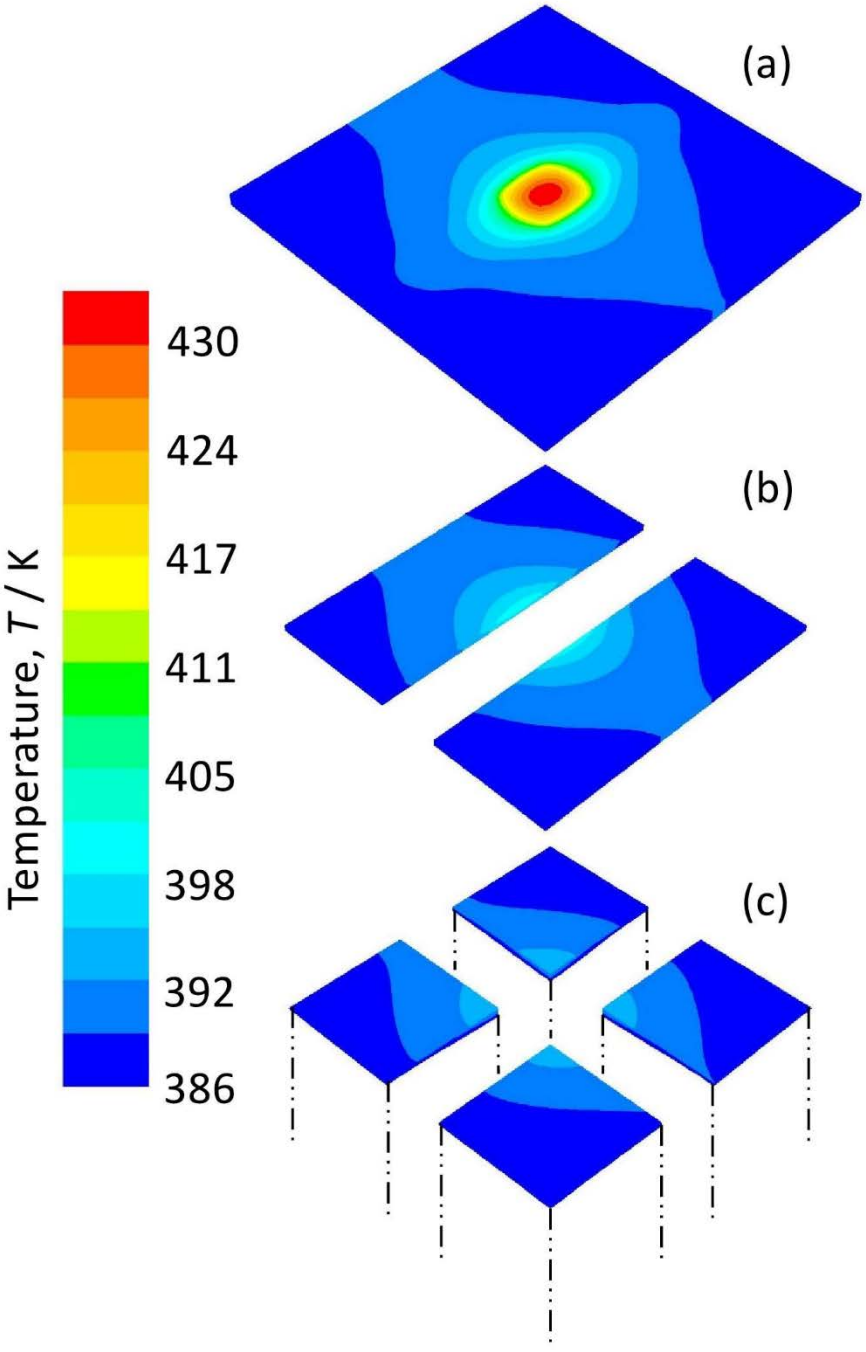

Fig.7 Temperature distributions on (a) top surface of alumina plate, (b) upper surface of electrodes, and (c) upper surfaces of TE elements, when the maximum output power generated at the model I.

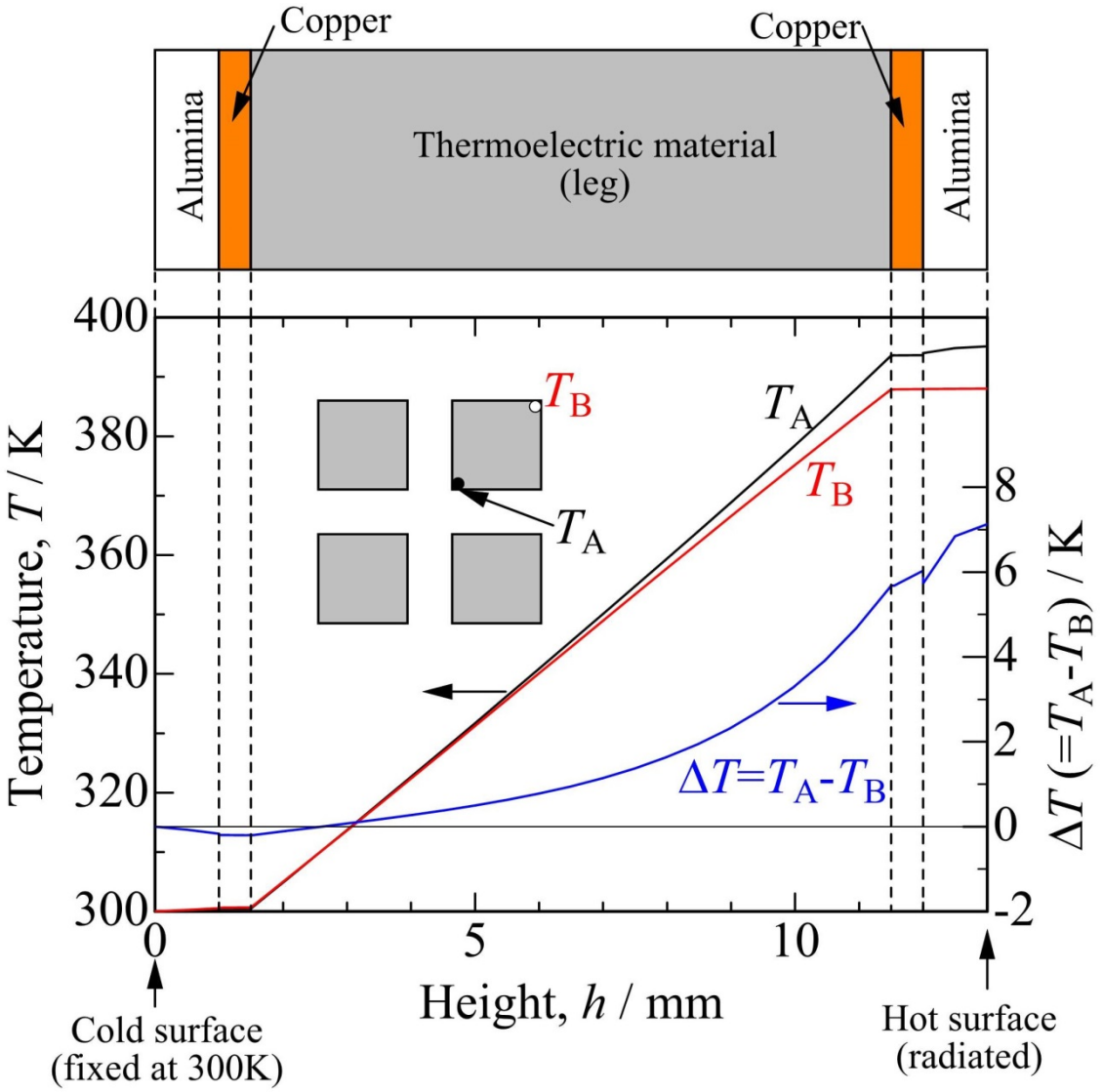

Fig.8 Temperature distributions on the two side edges of TE elements, when the maximum output power generated at the model I. T_A and T_B are the temperatures at the inner and outer edges (see Fig.7(c)), and the temperature difference between them, ΔT, is shown as a function of height.

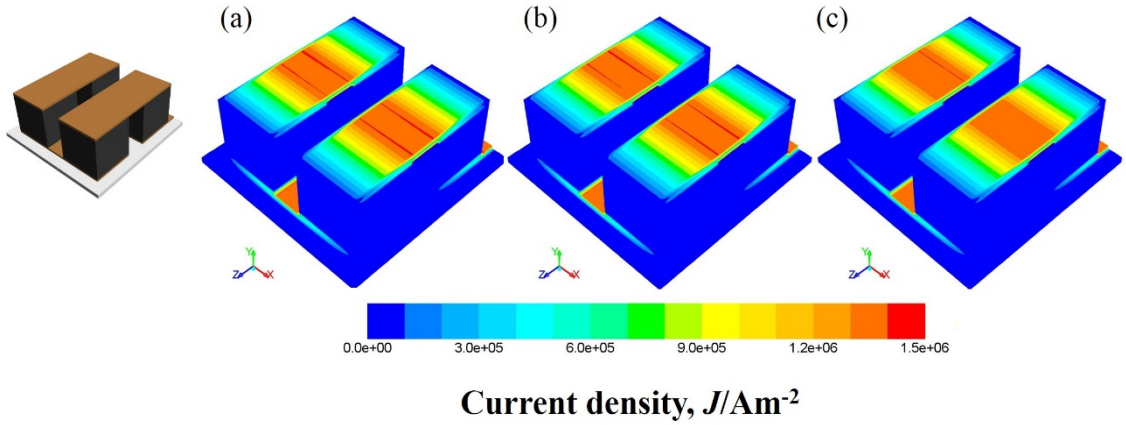

Fig.9 Profiles of current density when the maximum output powers generated. (a), (b) and (c) correspond to the model I, II and III, respectively.

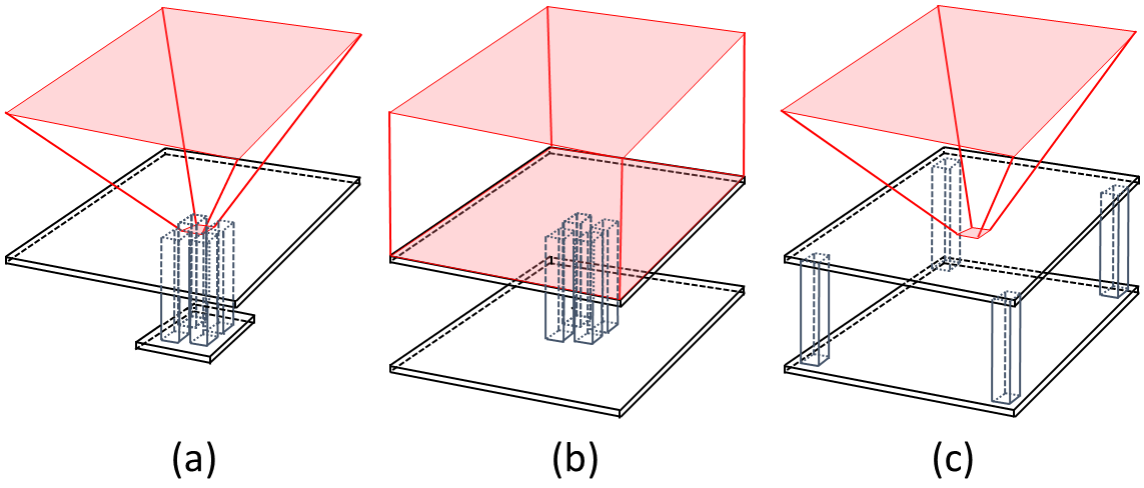

Fig.10 Illustration of TE modules for solar light power generation, where their maximum output powers are expected to be equivalent with the TE module as shown in Fig. 3(b). (a) the solar light is concentrated in a single point below which TE legs are installed, (b) it is radiated homogeneously without concentration, and (c) it is concentrated on a central point of the plate whose four corners are supported by TE legs.